

Simultaneous Inference of Neutron Star Equation of State and Hubble Constant with a Population of Merging Neutron Stars

Tathagata Ghosh ¹, Bhaskar Biswas ^{1,2} and Sukanta Bose^{1,3}

¹*Inter-University Centre for Astronomy and Astrophysics, Post Bag 4, Ganeshkhind, Pune 411 007, India*

²*The Oskar Klein Centre, Department of Astronomy, Stockholm University, AlbaNova, SE-10691 Stockholm, Sweden*

³*Department of Physics & Astronomy, Washington State University, 1245 Webster, Pullman, WA 99164-2814, U.S.A*

(Dated: July 19, 2022)

We develop a method for implementing a proposal on utilizing knowledge of neutron star (NS) equation of state (EoS) for inferring the Hubble constant from a population of binary neutron star (BNS) mergers. This method is useful in exploiting BNSs as standard sirens when their redshifts are not available. Gravitational wave (GW) signals from compact object binaries provide a direct measurement of their luminosity distances, but not their redshifts. Unlike in the past, here we employ a realistic EoS parameterization in a Bayesian framework to simultaneously measure the Hubble constant and refine the constraints on the EoS parameters. The uncertainty in the redshift depends on the uncertainties in the EoS and the mass parameters estimated from GW data. Combining the inferred BNS redshifts with the corresponding luminosity distances, one constructs a redshift-distance relation and deduces the Hubble constant from it. Here, we show that in the Cosmic Explorer era, one can measure the Hubble constant to a precision of $\lesssim 5\%$ (with a 90% credible interval) with a realistic distribution of a thousand BNSs, while allowing for uncertainties in their EoS parameters. Such a measurement can potentially resolve the current tension in the measurements of the Hubble constant from the early- and late-time universe. The methodology implemented in this work demonstrates a comprehensive prescription for inferring the NS EoS and the Hubble constant by simultaneously combining GW observations from merging NSs, while employing a simple population model for NS masses and keeping the merger rate of NSs constant in redshift. This method can be immediately extended to incorporate merger rate, population properties, and additional cosmological parameters.

I. INTRODUCTION

Gravitational Wave (GW) observations of compact binary coalescences (CBC) have opened a new era of precision cosmology. One of the key goals is to measure the Hubble constant (denoted by H_0), the current expansion rate of the Universe. GW allows the direct measurement of luminosity distance. Additionally, if the redshifts of GW sources are available from any other observations, the Hubble constant can be estimated from the distance-redshift relation. In the absence of an electromagnetic (EM) counterpart, the Hubble constant can be measured using statistical correlation [1–8] of distance with an ensemble of potential host galaxies within the GW event localization uncertainty region. The first ever multi-messenger detection of binary neutron star (BNS) merger GW170817 [9] by the Advanced LIGO [10] and Advanced Virgo detectors [11], with unique identification of host galaxy NGC 4993, is the first standard siren used for the measurement of the Hubble constant $H_0 = 70_{-8}^{+12}$ km s⁻¹ Mpc⁻¹ [12]. However, it is not clear what fraction of BNSs observed in GWs may have EM counterparts that yield a precise redshift measurement, especially at large distances. In this work, we make the conservative assumption that this fraction is small [12, 13].

Apart from bright sirens, like GW170817, H_0 can also be estimated from dark sirens, which lack confirmed EM counterparts. The LIGO-Virgo-KAGRA collaboration recently published the updated measure-

ments of the Hubble constant [14] using 47 GW events from GWTC-3 [15] to be 68_{-8}^{+12} km s⁻¹ Mpc⁻¹ and 68_{-6}^{+8} km s⁻¹ Mpc⁻¹ following two different methods, as described in Ref. [16] and Ref. [5], respectively. These recent measurements are clearly an improvement compared to the previous estimate of $H_0 = 69_{-8}^{+16}$ km s⁻¹ Mpc⁻¹ – from observations during the O1-O2 runs [17]. Unsurprisingly, all of these GW constraints on H_0 have significant contribution from the observations of GW170817 and its EM counterpart. More instances of independent measurements of luminosity distance and redshift from a wide distribution of sources would be useful toward a resolution of the current tension in H_0 measurements from the early and late-time universe [18]. To wit, there is a 4.4σ discrepancy between the values of H_0 as measured from the cosmic microwave background (67.36 ± 0.54 km s⁻¹ Mpc⁻¹ [19]) and observations based on the cosmic distance ladder comprising Cepheid variable stars and supernovae Type Ia (73.04 ± 1.04 km s⁻¹ Mpc⁻¹ [20]).

Messenger and Read [21] proposed an alternative idea of determining the redshift of a binary neutron star (BNS) merger in a GW observation by using prior knowledge of the neutron star (NS) equation of state (EoS). The phase $\Psi(f)$ of the frequency domain GW waveform, $\tilde{h}(f) = A(f)e^{-i\Psi(f)}$ (where $A(f)$ is the amplitude of GW waveform at frequency f), has two components: one of them is the standard post-Newtonian point-particle frequency domain phase $\Psi_{\text{PP}}(f)$ and the other is the phase component $\Psi_{\text{tidal}}(f)$ due to the tidal deformability of the

neutron star, i.e., $\Psi(f) = \Psi_{\text{PP}}(f) + \Psi_{\text{tidal}}(f)$. Ψ_{PP} depends on redshifted chirp-mass and luminosity distance. Moreover, in contrast to Ψ_{tidal} the phase Ψ_{PP} is redshift invariant [21]. The degeneracy between the mass parameters and the redshift can be broken if one knows the EoS of NSs. This technique is especially useful when the BNS is not accompanied by an electromagnetic counterpart to infer redshift directly. This method neither depends on the observation of EM counterpart nor the identification of potential host galaxies for statistical cross-correlation methods.

Recent progress was reported by Chatterjee *et al.* [22] by building on the basic concept proposed in Ref. [21]. Their key idea was to use binary Love relations [23] to capture information about NS EoS in a single tidal parameter and use it to constrain the Hubble constant. In this work, we too follow Ref. [21] but use a Hybrid Nuclear plus piecewise-polytrope (PP) parameterization to model the NS EoS [24, 25]. Specifically, at low densities in the star the nuclear empirical parameters are used to construct the EoS model. These nuclear empirical parameters (*e.g.*, nuclear symmetry energy) can be constrained from laboratory experiments and astrophysical observation of neutron stars. The NS EoS, however, is less well understood at densities that are about a couple of times the nuclear saturation density or higher. In those regions, we use the three-piece PP model. We will briefly discuss the EoS model in the next section.

The structure of the paper is as follows. Sec. II introduces the construction of the EoS model. In Section III, we describe the Bayesian framework to infer the Hubble constant. In Secs. IV and V, we discuss the required simulations and the results, respectively. For our simulations, we take the Λ CDM cosmology with $\Omega_m = 0.3$ and $H_0 = 70 \text{ km s}^{-1} \text{ Mpc}^{-1}$ as the *true* cosmology throughout.

II. EOS MODEL: HYBRID NUCLEAR+PP

In this section, we briefly introduce hybrid nuclear+PP EoS parameterization, which has been used in the past [24, 25] to put joint GW-electromagnetic constraints on the properties of neutron stars. This hybrid EoS parameterization is also used to investigate the nature of the ‘‘mass-gap’’ object in GW190814 [26]. Since the crust has minimal impact [27, 28] on the macroscopic properties of NSs such as mass, radius, tidal deformability, etc., standard BPS EoS [29] is used to model the crust under this parameterization. Then this fixed crust is joined with the core EoS in a thermodynamically consistent fashion described in Ref. [30]. The core EoS is divided into two parts:

1. EoS around the nuclear saturation density (ρ_0) is well described via the parabolic expansion of energy per nucleon

$$e(\rho, \delta) \approx e_0(\rho) + e_{\text{sym}}(\rho)\delta^2, \quad (1)$$

where $e_0(\rho)$ is the energy of symmetric nuclear matter for which the number of protons is equal to the number of neutrons, e_{sym} is the energy of the asymmetric nuclear matter (commonly referred as ‘symmetry energy’ in literature), and $\delta \equiv \frac{\rho_n - \rho_p}{\rho_p + \rho_n}$ (where ρ_n, ρ_p being the number density of neutron and proton respectively) is the measure of asymmetry in the number density of neutrons and protons. Around ρ_0 , these two energies can be further expanded in a Taylor series:

$$e_0(\rho) = e_0(\rho_0) + \frac{K_0}{2}\chi^2 + \dots, \quad (2)$$

$$e_{\text{sym}}(\rho) = e_{\text{sym}}(\rho_0) + L\chi + \frac{K_{\text{sym}}}{2}\chi^2 \dots, \quad (3)$$

where $\chi \equiv (\rho - \rho_0)/3\rho_0 \ll 1$. We truncate the Taylor expansion up to the second order in χ as we use this expansion only up to $1.25\rho_0$. The lowest order parameters are experimentally well constrained and therefore, we fix them at their median values such as $e_0(\rho_0) = -15.9 \text{ MeV}$, and $\rho_0 = 0.16 \text{ fm}^{-3}$. Therefore, the free parameters of this nuclear-physics informed model are the curvature of symmetric matter K_0 , nuclear symmetry energy e_{sym} , slope L , and curvature of symmetric energy K_{sym} . A survey based on 53 experimental results performed in 2016 [31] found of values of $e_{\text{sym}}(\rho_0) = 31.7 \pm 3.2 \text{ MeV}$ and $L = 58.7 \pm 28.1 \text{ MeV}$.

2. At higher densities, i.e., above $1.25\rho_0$, empirical parameterization starts to break down and we use a three-piece piecewise-polytrope (Γ_1, Γ_2 , and Γ_3 are being the polytropic indices) parameterization divided by the fixed transition densities at $10^{14.7} \text{ gm/cm}^3$ and 10^{15} gm/cm^3 respectively.

Instead of using all the EoS parameters explicitly, we will generally use $\mathcal{E} = \{K_0, e_{\text{sym}}, L, K_{\text{sym}}, \Gamma_1, \Gamma_2, \Gamma_3\}$. In our work, we consider this particular EoS model to constrain the cosmological parameters. In the future, different choices of EoS parameterization or even an EoS-insensitive approach [32] can be explored for applying this methodology.

III. METHODOLOGY

Gravitational-wave observations of the leading binary phase terms, in Ψ_{PP} , provide mass estimation in the detector-frame; i.e., the source-frame mass m is observed as redshifted mass, defined as $m^z = m(1+z)$, where z is the redshift of the source. Contrastingly, tidal deformability measurements of a BNS merger in GW observations depend on the source-frame mass pair. Since the detector-frame masses are well estimated from post-Newtonian (PN) terms at lower orders, tidal deformability can provide the redshift information if we know the NS EoS [21]. The redshift of the BNS, so obtained, can be combined with its luminosity distance to infer the Hubble constant. However, it has proved quite challenging to measure the NS EoS very precisely. While it is fair to expect that it will be better constrained by the time of

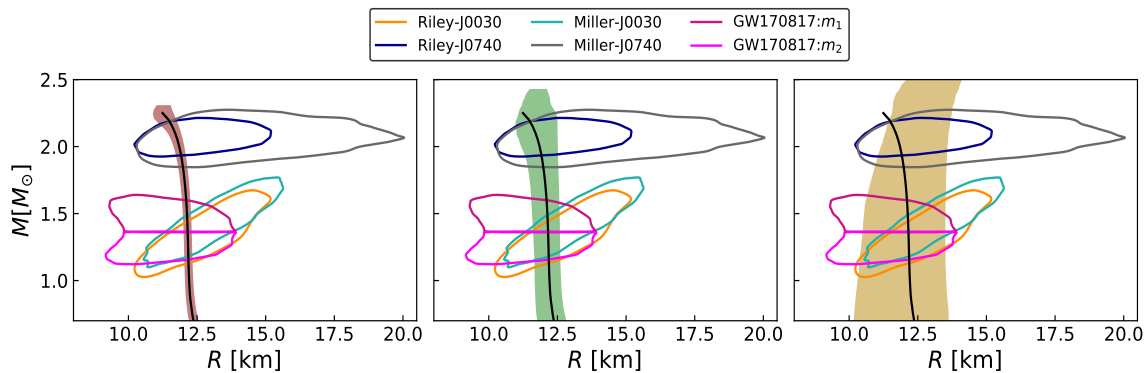


FIG. 1. 90% credible interval of mass-radius priors are shown corresponding to three different choices of EoS prior distributions, as described in Table I. The solid black line corresponds to the injected EoS.

TABLE I. Different choices of uncertainties in EoS parameters that we use to establish the effectiveness of our method, as described in Sec. II. Here $\mathcal{N}(\mu, \sigma)$ refers to the Gaussian distribution with mean μ and standard deviation σ .

EoS Parameters	Injected	Prior 1	Prior 2	Prior 3
K_0 [MeV]	240	$\mathcal{N}(240, 2.5)$	$\mathcal{N}(240, 20)$	$\mathcal{N}(240, 30)$
e_{sym} [MeV]	31.7	$\mathcal{N}(31.7, 0.5)$	$\mathcal{N}(31.7, 2.5)$	$\mathcal{N}(31.7, 3.2)$
L [MeV]	58.7	$\mathcal{N}(58.7, 1.5)$	$\mathcal{N}(58.7, 5)$	$\mathcal{N}(58.7, 28.1)$
K_{sym} [MeV]	-100	$\mathcal{N}(-100, 2.5)$	$\mathcal{N}(-100, 50)$	$\mathcal{N}(-100, 100)$
Γ_1	2.5	$\mathcal{N}(2.5, 0.05)$	$\mathcal{N}(2.5, 0.2)$	$\mathcal{N}(2.5, 0.5)$
Γ_2	3.5	$\mathcal{N}(3.5, 0.05)$	$\mathcal{N}(3.5, 0.2)$	$\mathcal{N}(3.5, 0.5)$
Γ_3	3.0	$\mathcal{N}(3.0, 0.5)$	$\mathcal{N}(3.0, 2.0)$	$\mathcal{N}(3.0, 2.5)$

the third generation GW detectors, e.g., Cosmic Explorer (CE) [33] and Einstein Telescope (ET) [34], nevertheless there will always be some uncertainty present in the values of the EoS parameters even in that era [33, 34]. We outline a Bayesian framework for inferring the cosmological parameters from GW observations of BNSs with (imprecise) knowledge of NS EoS. We allow for realistic

uncertainties in the values of the EoS parameters and assign corresponding priors to them. These priors are then utilized to infer H_0 and simultaneously refine the constraints on the NS EoS parameters. Indeed, the joint posterior of the Hubble constant and the NS EoS parameters is given by

$$\begin{aligned}
 p(H_0, \mathcal{E} | \{x_{\text{GW}}\}) \propto & \prod_{i=1}^{N_{\text{det}}} \frac{\pi(H_0)}{\beta(H_0)} \pi(\mathcal{E}) \iiint p(x_{\text{GW}_i} | m_1^z(m_1, z), m_2^z(m_2, z), \Lambda_1(m_1, \mathcal{E}), \Lambda_2(m_2, \mathcal{E}), d_L(z, H_0)) \\
 & \times \pi(m_1, m_2 | \mathcal{E}) \pi(z) dz dm_1 dm_2,
 \end{aligned} \tag{4}$$

where x_{GW} is the GW data, $m_{1,2}^z$ are the detector-frame (redshifted) masses of a BNS corresponding to the source-frame masses $m_{1,2}$ at redshift z , $\Lambda_{1,2}$ are the tidal deformabilities, and d_L is the luminosity of the source (which is related to its z , via the Hubble constant H_0). Here, $\pi(H_0)$, $\pi(\mathcal{E})$ and $\pi(z)$ are the prior distributions over the Hubble constant, EoS parameters and redshift, respectively. $\pi(m_1, m_2 | \mathcal{E})$ is the prior distribution over the source-frame component masses determined from the

NS population model and the choice of EoS parameters \mathcal{E} . $\beta(H_0)$ is a normalization factor, which ensures that the GW likelihood factor $p(x_{\text{GW}} | m_1^z, m_2^z, \Lambda_1, \Lambda_2, d_L)$ integrated over all observable sources is unity. A detailed derivation of the Bayesian framework is described in Appendix A.

In our work, the mass distribution of NS is chosen to be uniform as follows:

$$p_{\text{pop}}(m | \mathcal{E}) = \begin{cases} \frac{1}{m_{\text{max}}(\mathcal{E}) - m_{\text{min}}}, & \text{iff } m_{\text{min}} \leq m \leq m_{\text{max}} \\ 0, & \text{otherwise,} \end{cases} \quad (5)$$

where m_{min} is the minimum mass and m_{max} is the maximum mass for the particular EoS parameters \mathcal{E} . Specifically, in our population model the BNS mass distribution is taken as:

$$\pi(m_1, m_2 | \mathcal{E}) \propto p_{\text{pop}}(m_1 | \mathcal{E}) p_{\text{pop}}(m_2 | \mathcal{E}), \quad (6)$$

subject to the constraint $m_1 \geq m_2$.

In Eq. (4), the prior over the redshift of the source is represented by $\pi(z)$, taken to be of the form

$$\pi(z) \propto \frac{dV_c}{dz} \frac{R(z)}{1+z}. \quad (7)$$

Here, $V_c(z)$ is the comoving volume as a function of redshift, and $R(z)$ is the merger-rate density in the detector-frame. The factor $(1+z)^{-1}$ above converts the merger rate from the source-frame time to the detector-frame time. In general, the merger rate density may be a function of redshift. In our work, we consider $R(z)=\text{constant}$, i.e., the BNS distribution is considered to be uniform in comoving volume and source-frame time throughout this work. The prior over the Hubble constant $\pi(H_0)$ is chosen to be uniform. The prior ranges of all the relevant parameters are mentioned in Sec. IV.

The GW likelihood factor $p(x_{\text{GW}} | m_1^z, m_2^z, \Lambda_1, \Lambda_2, d_L)$ in Eq. (4) denotes the probability that the GW data contains a signal from a BNS merger (with parameters $m_{1,2}^z$, $\Lambda_{1,2}$ and d_L), marginalized over the complementary set of signal parameters. Using the Bayes theorem, the posterior for $(m_1^z, m_2^z, \Lambda_1, \Lambda_2, d_L)$ can be written as:

$$p(m_1^z, m_2^z, \Lambda_1, \Lambda_2, d_L | x_{\text{GW}}) \propto p(x_{\text{GW}} | m_1^z, m_2^z, \Lambda_1, \Lambda_2, d_L) \times \pi(m_1^z, m_2^z, \Lambda_1, \Lambda_2, d_L), \quad (8)$$

where $\pi(m_1^z, m_2^z, \Lambda_1, \Lambda_2, d_L)$ is the prior distribution used to produce the posterior of GW signal parameters. To obtain the likelihood from the posterior probability, we have to divide out the *prior* $\pi(m_1^z, m_2^z, \Lambda_1, \Lambda_2, d_L)$. We have taken uniform priors over $\Lambda_{1,2}$, the chirp-mass in the detector frame $\mathcal{M}_c^z = \frac{(m_1 m_2)^{3/5}}{(m_1 + m_2)^{1/5}}(1+z)$, and the mass-ratio $q = m_2/m_1$ while estimating the GW signal parameters. The prior for luminosity distance is uniform in the comoving volume. The prior $\pi(m_1^z, m_2^z, \Lambda_1, \Lambda_2, d_L)$ is thus simplified as

$$\pi(m_1^z, m_2^z, \Lambda_1, \Lambda_2, d_L) \propto \pi(m_1^z) \pi(m_2^z) \pi(d_L). \quad (9)$$

Since we have considered observed component mass pair $(m_{1,2}^z)$ of BNS in our Bayesian analysis in Eq. (4), we have to compute the relevant prior distribution over the component observed mass-pair ($\pi(m_1^z)$ and $\pi(m_2^z)$ in Eq. (9)) corresponding to uniform priors over \mathcal{M}_c^z and q used for constraining the GW signal parameters.

In Eq. (4), the normalization term $\beta(H_0)$ encodes the selection effect [2, 35]; it is defined as:

$$\beta(H_0) = \int p_{\text{det}}(z, H_0) \pi(z) dz, \quad (10)$$

where p_{det} denotes the detection probability of any GW event. In Appendix B we describe how p_{det} is computed in our simulations.

When quantifying the selection effect, we should ideally consider the effect of the uncertainty in the NS EoS parameters and the population of BNSs since p_{det} depends on the properties of the GW source population. The uncertainty in EoS parameters also affects the mass distribution, as maximum mass depends on the values of EoS parameters. The effect of tidal deformability on the amplitude of the gravitational wave signal is small [36, 37]. So, we have fixed the EoS parameters at the injection values and, hence, have also fixed the maximum mass ($\approx 2.27M_\odot$) to correspond to injected EoS parameters. For simplicity, we assume that the population properties are known exactly. However, it will be a good exercise to include the uncertainties in the properties of the GW source population in a future work. We prepare the mock GW catalog assuming that the masses of BNSs follow a uniform distribution in the source frame such that $m_1 \geq m_2$ (see, Eq. 6). It is clear from Eq. (5) that the population of BNS depends on the minimum and maximum mass of BNS. The minimum and maximum mass are fixed in the simulation. However, the maximum mass is determined by the EoS of NS. Since we do not account for the uncertainty of EoS parameters for estimating the selection effect, the maximum mass is also fixed (to the value mentioned above). So, the population of BNS does not affect the selection effect.

We assumed flat Λ CDM cosmology with H_0 as a free parameter while performing our Bayesian formulation, Eq. (4). In flat Λ CDM universe, the luminosity distance d_L is related to redshift z as

$$d_L(z) = \frac{c(1+z)}{H_0} \int_0^z \frac{dz'}{\sqrt{\Omega_m(1+z')^3 + (1-\Omega_m)}}. \quad (11)$$

We have used `PyMultiNest`¹ [38], python based package based on the nested sampling algorithm `Multinest` to perform the parameter estimation within the Bayesian framework as mentioned in Eq. (4). During this Bayesian analysis, we use the multivariate Gaussian kernel density estimator from `statsmodels`² [39] to calculate the GW likelihood term.

¹ <https://johannesbuchner.github.io/PyMultiNest/>

² <https://www.statsmodels.org/>

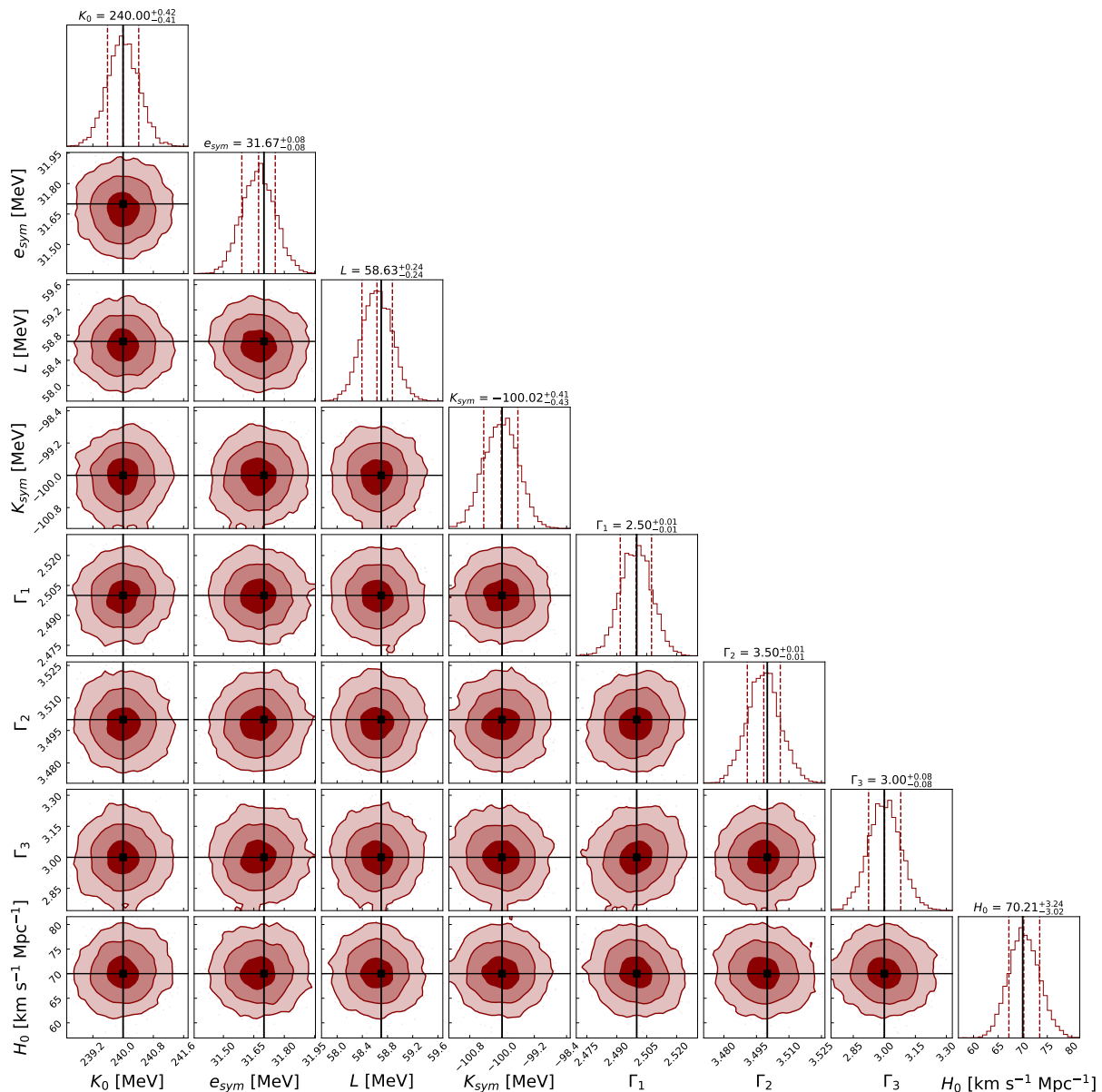


FIG. 2. Constraint on the EoS parameters and H_0 by combining 50 GW events as detected by CE using EoS Prior 1. The black lines show the injected values. The median and 1σ credible intervals are also shown in the respective marginalized one-dimensional posterior.

IV. SIMULATION

We test the method described in Sec. III on several simulated GW events. We first created a mock GW catalog by injecting the sources uniformly over the sky. The redshift distribution of the sources follows Eq. (7), with $R(z)=\text{constant}$ and d_L between 100Mpc and 8Gpc. The masses of the BNS mergers follow uniform distribution in the source frame, as mentioned in Eq. 6, where $m_{\min} = 1M_{\odot}$ and $m_{\max} = 2.27M_{\odot}$. However, the uniform prior in source-frame mass is not a realistic mass distribution [40]. We consider a uniform distribution over the source-frame mass for simplicity. However, it

will be worth applying this methodology in the future to different population models of BNS to understand the effect of the population on the simultaneous measurement of the Hubble constant and the EoS parameters. We consider flat Λ CDM cosmology with $\Omega_m = 0.3$ and $H_0 = 70 \text{ km s}^{-1} \text{ Mpc}^{-1}$ to determine the redshift of the GW sources from their luminosity distances. We ignore the spins of neutron stars (set to 0) in the present work.

Tidal deformability of a neutron star depends on its mass, given a particular EoS. The injected values of the EoS parameters are $K_0 = 240 \text{ MeV}$, $e_{\text{sym}} = 31.7 \text{ MeV}$, $L = 58.7 \text{ MeV}$ and $K_{\text{sym}} = -100 \text{ MeV}$, $\Gamma_1 = 2.5$, $\Gamma_2 = 3.5$ and $\Gamma_3 = 3.0$. In Fig. 1, we show the injected

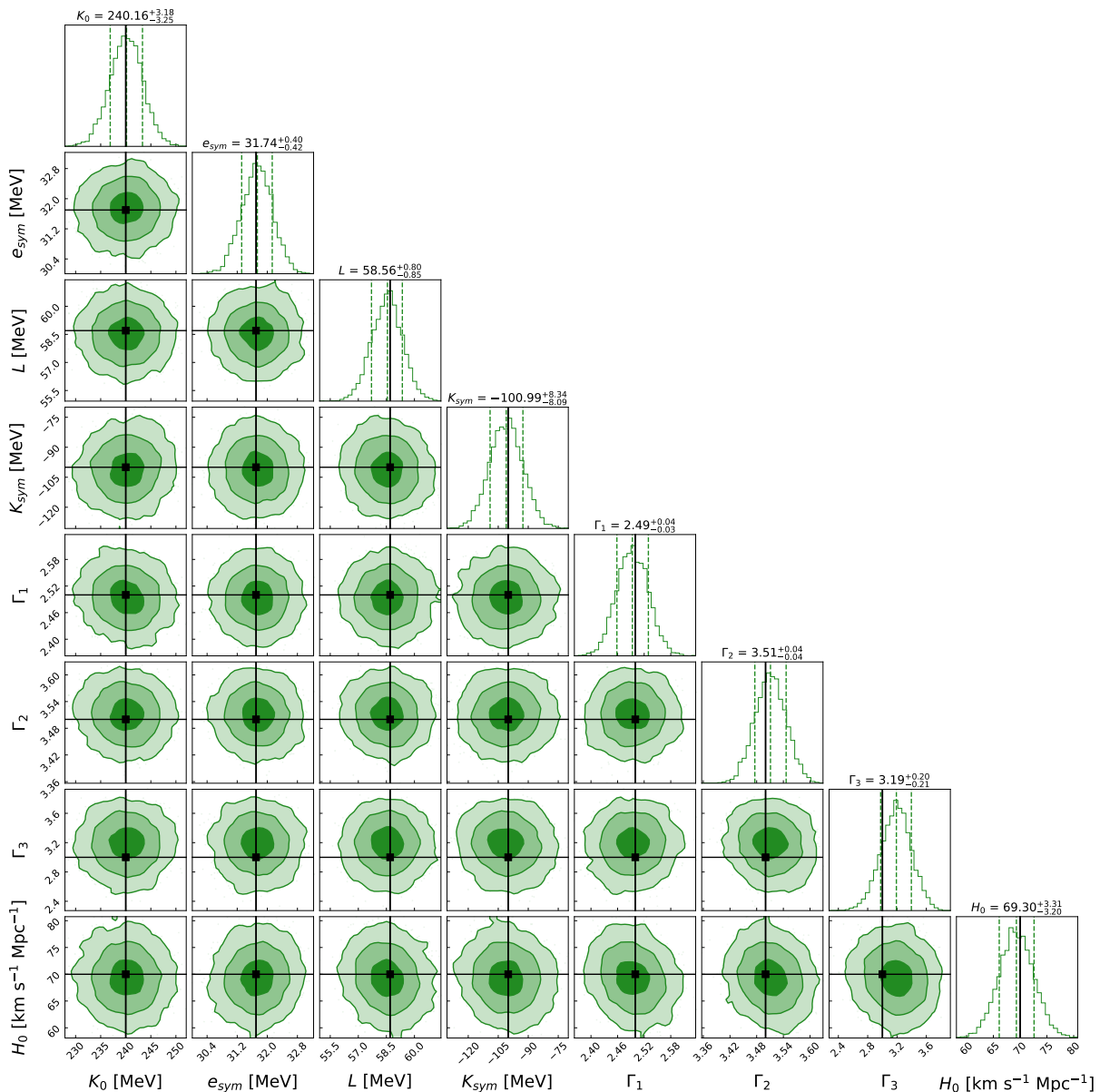


FIG. 3. Same as in Fig. 2 but now using EoS Prior 2.

EoS, which is consistent with the constraints on the mass-radius measurement from PSR J0030+0451 [41, 42] and PSR J0740+6620 [43, 44] by the NICER collaboration; and GW170817 by LIGO-Virgo observations [45]. We consider CE as the detector in our simulation. We inject a synthetic BNS signal, of 128 sec duration, in stationary Gaussian noise with CE sensitivity³ [46]. Though CE will observe a much longer signal, the tidal effect, which begins at 5PN, is more pronounced closer to the merger [21, 22]. We consider the same waveform model IMRPhenomPv2_NRTidal [47] for both signal injection and

recovery. We used `bilby_pipe`⁴, a package for automating the process of running `bilby`⁵ [48] for gravitational wave parameter estimation in computing clusters, to estimate the posterior of the parameters of BNS signals. We performed parameter estimation over the mass pair, tidal deformabilities, luminosity distance and inclination angle. For mass estimation, we consider uniform prior over observed chirp-mass (in the range $\mathcal{M}_{c,\text{inj}}^z \pm 0.1 M_{\odot}$) and mass-ratio $q = m_2/m_1 \in [0.2, 1]$. We use a uniform prior in tidal deformabilities $\Lambda_{1,2} \in [0, 5000]$. For

³ <https://dcc.ligo.org/LIGO-T1500293/public>

⁴ <https://pypi.org/project/bilby-pipe/>

⁵ <https://lscsoft.docs.ligo.org/bilby/>

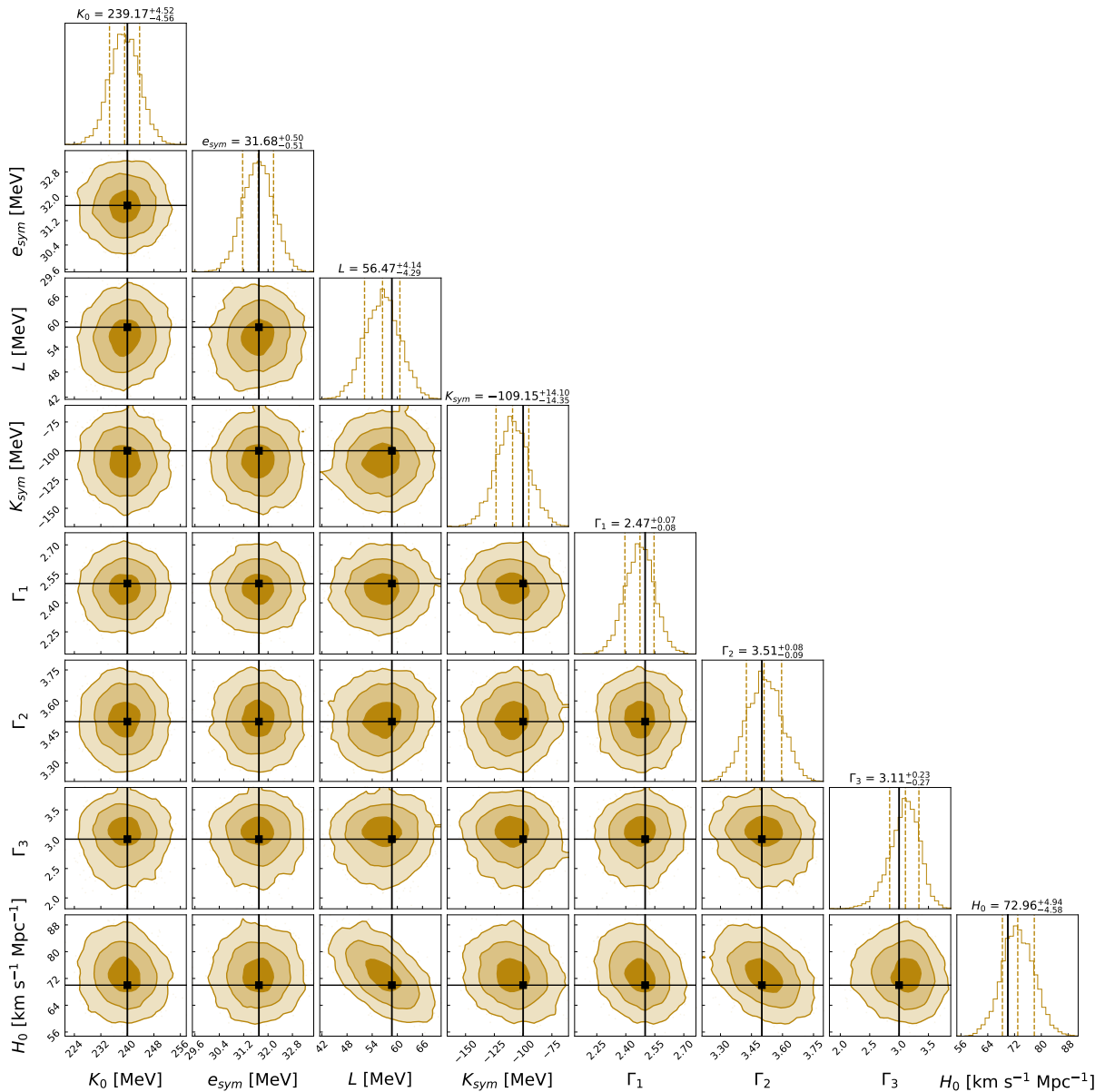


FIG. 4. Same as in Fig. 2 but now using EoS Prior 3.

estimating the luminosity distance, we choose the prior in the comoving distance to be uniform and between 10 Mpc and $2d_{L,\text{inj}}$. We consider isotropic prior over to infer the inclination angle. We fixed the remaining parameters (namely, sky-position, dimensionless spin magnitudes, tilt angle between their spins, orbital angular momentum, spin vectors describing the azimuthal angle separating the spin vectors, precession angle, polarization angle, coalescence time and its orbital phase at coalescence) at the injected values.

Now, the parameters of the synthetic GW catalog have been used to determine H_0 and the EoS parameters, as discussed in Sec. III. We consider sufficiently large uniform prior over redshift to cover the entire luminosity distance posterior obtained from GW observa-

tion for any value of H_0 within our prior range between $10 \text{ km s}^{-1} \text{ Mpc}^{-1}$ and $300 \text{ km s}^{-1} \text{ Mpc}^{-1}$. We have already mentioned that we need to assume some uncertainty in the EoS parameters. The projected uncertainty in $R_{1.4}$ measurement is $\sim 1 \text{ km}$ after the fifth observing (O5) run of LIGO-Virgo-KAGRA network [49]. The constraint on the NS radius is expected to be better than 0.1 km from BNS observations by the time of CE [33]. So, we consider three sets of uncertainties in the EoS parameters, mentioned in Table I along with the injected values of the EoS parameters. The mass-radius plot for all the prior EoSs, shown in Fig. 1 gives a similar qualitative measurement about the uncertainties in the EoS parameters we are considering in our work. Now, the posterior of Hubble constant along with the EoS parameters

have been measured using the redshift information and luminosity distance of GW sources using the Bayesian framework as described above.

V. RESULTS

We apply the method described in Sec. III to 50 GW events to test its efficacy in estimating the EoS parameters and the Hubble constant simultaneously. We consider a simulated GW signal as detected if its network SNR turns out to be equal to or greater than 8. The individual posteriors of the EoS parameters and the Hubble constant may not always be peaked at the true values; some posteriors may be multi-modal as well. In particular, there exists a degeneracy in the measurability of the luminosity distance and the inclination angle of binaries in GWs [50, 51]; e.g., a source will appear fainter not just when it is farther but also when its orbital plane is more tilted relative to the line of sight (see Ref. [2]). Since the orbit orientations in a population are random, the expectation is that with an increasing number of observations, this method of combining individual source parameter posteriors will still succeed in constraining H_0 and the EoS parameters with increasing precision since every BNS signal is characterized by the same H_0 and the EoS parameters.

The combined posteriors of the inferred EoS parameters and H_0 , together with their correlation, are shown in Figs. 2, 3 and 4 corresponding to Priors 1, 2 and 3, respectively. The different choices of priors in the EoS parameters (also discussed in Sec. IV) are mentioned in Table I. We summarize the 90% credible interval of the inferred EoS parameters and Hubble constant in Table II. We also mention some other inferred parameters from the NS EoS posteriors like $R_{1.4M_\odot}$ (radius of neutron star at $1.4M_\odot$), R_{2M_\odot} , $\Lambda_{1.4M_\odot}$ (tidal deformability of neutron star at $1.4M_\odot$) and Λ_{2M_\odot} in Table II.

From the joint posterior of H_0 and the EoS parameters (see Fig. 2, 3 and 4 and Table II), it is evident that the uncertainty in measurement of the Hubble constants using EoS Priors 1 and 2 are not significantly different (see Fig. 6). In comparison, the posterior of the Hubble constant estimated using EoS Prior 3 is slightly broad. However, the uncertainties in the posterior of the EoS parameters are quite different: To wit, a tighter prior of the EoS parameters leads to narrower EoS parameter posteriors. The mass-radius plots (see Fig. 5 and Table II for the median values with the 90% credible intervals of EoS parameters) corresponding to three EoS posteriors also reveal that the constraints of the EoS parameters are significantly different.

We have also studied the (fractional) uncertainty in inferring the redshift and the Hubble constant with BNSs (with source-frame masses $(1.4+1.26)M_\odot$) as functions of the luminosity distances. The results are shown in Fig. 8. The uncertainty in H_0 saturates at large distances. It is important to note that the errors in the various observ-

ables (such as the redshift, luminosity distance and the Hubble constant in Fig. 8) vary from one GW event to another depending on their intrinsic and extrinsic parameters. However, the qualitative trends in the error plots are expected to be similar for the same GW source at different distances when the other parameters are kept fixed.

Most of the sources in the population of BNSs used in this work are at large distances since they are distributed uniformly in comoving volume and source-frame time. Hence, the estimation of the Hubble constant is not sensitive to the EoS parameters' uncertainty for the injected population. We can also expect some improvement in the mitigation of the well-known distance-inclination degeneracy with the development of the higher-mode waveform models for BNSs [52], thereby aiding a more precise estimation of the Hubble constant.

Chatterjee *et al.* [22] mentioned that $\Delta H_0/H_0 \sim 2\%$ for $N_{\text{det}} = 10^3$ detected GW events observed by CE. They assumed $\sim 1/\sqrt{N_{\text{det}}}$ scaling for estimating the projected uncertainty measurement in the Hubble constant during CE era. We find the 90% credible interval error $\Delta H_0/H_0 \lesssim 15 - 22\%$ (see Fig. 6), depending on the prior EoS, while inferring the Hubble constant from 50 BNS observations. We also estimate the uncertainty with a similar scaling $\sim 1/\sqrt{N_{\text{det}}}$ in the measurement of the Hubble constant $\Delta H_0/H_0 \lesssim 3 - 5\%$ with $N_{\text{det}} = 10^3$ events, depending on the uncertainties in the EoS parameters. The projected uncertainty in H_0 measurement is slightly greater than the uncertainty estimation of H_0 , mentioned by Chatterjee *et al.* [22]. It is expected because we consider uncertainties in the EoS parameters, unlike Chatterjee *et al.* [22]. However, improvement in the uncertainty due to luminosity distance-inclination angle degeneracy should have a more significant effect in constraining H_0 as discussed above.

Recently, PREX-II collaboration have reported [53] the value of neutron skin thickness of ^{208}Pb to be, $R_{\text{skin}}^{208} = 0.29 \pm 0.07$ fm (mean and 1σ standard deviation). Ref. [54] have argued, this result implies the value of L to be 106 ± 37 MeV. They also deduce a larger value of NS radius as there exist a correlation between $R_{1.4}$ and L based on relativistic mean field calculation. However, Ref. [25] argued that the measurement uncertainty in R_{skin}^{208} by PREX-II is quite broad; Moreover, the measurement uncertainty deduced after addition of astrophysical observations is dominated by the latter. Combined astrophysical observations and PREX-II data yields the value of empirical parameter $L = 69_{-19}^{+21}$ MeV, $R_{\text{skin}}^{208} = 0.20_{-0.05}^{+0.05}$ fm, and radius of a $1.4M_\odot$ ($R_{1.4}$) = $12.70_{-0.54}^{+0.42}$ km at 1σ credible interval. Nevertheless, a better measurement of R_{skin}^{208} might have a small effect on the radius of low mass NSs, but for the high masses there will be almost no effect. The state-of-the-art chiral effective field theory calculations predict [55] the value of R_{skin} to be $0.17 - 0.18$ fm based on Bayesian analyses using mocked data. Therefore, if the high R_{skin}^{208} values continue to persist with lesser uncer-

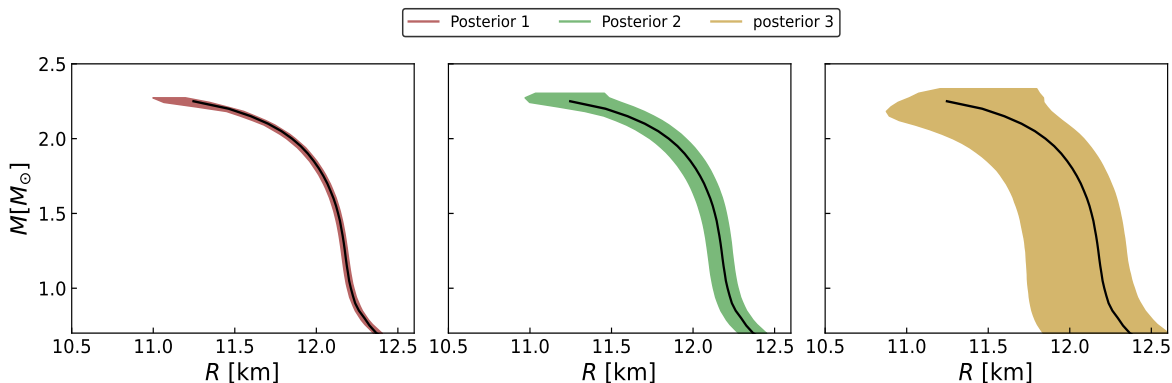


FIG. 5. 90% credible interval of mass-radius posteriors are shown using three different choices of the EoS prior distributions as mentioned in Table I. The solid black curve in each plot is the mass-radius plot corresponding to the injected EoS parameters.

TABLE II. Median and 90% credible interval of the EoS Parameters, $R_{1.4}$, R_2 , $\Lambda_{1.4}$, Λ_2 , M_{\max} , skin thickness and Hubble constant as obtained using our methodology to 50 GW events with EoS Prior 1, Prior 2 and Prior 3, mentioned in Table I. The parameters, such as $R_{1.4}$, R_2 , M_{\max} and skin thickness have been inferred from the injected EoS parameters (K_0 , e_{sym} , L , K_{sym} , Γ_1 , Γ_2 , Γ_3).

EoS Parameters	Injected	Posterior 1	Posterior 2	Posterior 3
K_0 [MeV]	240	$240.00^{+0.69}_{-0.69}$	$240.16^{+5.30}_{-5.51}$	$239.17^{+7.52}_{-7.45}$
e_{sym} [MeV]	31.70	$31.67^{+0.13}_{-0.13}$	$31.74^{+0.68}_{-0.69}$	$31.68^{+0.82}_{-0.82}$
L [MeV]	58.70	$58.63^{+0.40}_{-0.39}$	$58.56^{+1.33}_{-1.39}$	$56.47^{+6.77}_{-6.76}$
K_{sym} [MeV]	-100	$-100.02^{+0.67}_{-0.69}$	$-100.99^{+13.65}_{-13.65}$	$-109.15^{+23.79}_{-24.19}$
Γ_1	2.5	$2.50^{+0.01}_{-0.01}$	$2.49^{+0.06}_{-0.06}$	$2.47^{+0.12}_{-0.13}$
Γ_2	3.5	$3.50^{+0.01}_{-0.01}$	$3.51^{+0.06}_{-0.06}$	$3.51^{+0.14}_{-0.14}$
Γ_3	3.0	$3.00^{+0.13}_{-0.13}$	$3.19^{+0.34}_{-0.36}$	$3.11^{+0.36}_{-0.47}$
$R_{1.4M_\odot}$ [km]	12.153	$12.151^{+0.019}_{-0.019}$	$12.145^{+0.077}_{-0.077}$	$12.029^{+0.297}_{-0.321}$
R_{2M_\odot} [km]	11.851	$11.847^{+0.026}_{-0.027}$	$11.851^{+0.107}_{-0.114}$	$11.713^{+0.372}_{-0.439}$
$\Lambda_{1.4M_\odot}$	375.813	$379.829^{+6.469}_{-6.266}$	$378.997^{+17.064}_{-16.702}$	$357.726^{+55.797}_{-51.555}$
Λ_{2M_\odot}	29.33	$29.243^{+0.570}_{-0.585}$	$29.419^{+2.392}_{-2.404}$	$26.901^{+7.506}_{-7.335}$
M_{\max} [M_\odot]	2.271	$2.267^{+0.008}_{-0.011}$	$2.247^{+0.041}_{-0.069}$	$2.221^{+0.092}_{-0.092}$
R_{skin} [fm]	0.1873	$0.1872^{+0.0006}_{-0.0006}$	$0.1871^{+0.0019}_{-0.0020}$	$0.1840^{+0.0099}_{-0.0099}$
H_0 [km/s/Mpc]	70	$70.21^{+5.37}_{-4.95}$	$69.30^{+5.42}_{-5.35}$	$72.96^{+8.10}_{-7.84}$

tainty, it would pose a challenge to the current theoretical understanding about the nuclear matter near the saturation densities. Following Ref. [25] we estimate the skin thickness R_{skin} using the universal relation from Viñas *et al.* [56] connecting R_{skin} and the empirical parameter L : R_{skin}^{208} [fm] = $0.101 + 0.00147 \times L$ [MeV]. The estimation of skin thickness for the different EoS priors are shown in Fig. 7 and Table II. We find irrespective of the choice in the EoS priors, future observations from CE will constrain R_{skin} with sub-percentage precision. So if indeed there is a tension between nuclear theory and astrophysical observations, it will be revealed.

VI. DISCUSSION

In this paper, we demonstrate how a population of BNS can constrain the EoS parameters and the Hubble constant simultaneously during 3rd generation detector era when unique transient electromagnetic counterparts cannot be identified. For dark GW signal from CBC, the current state of the art is to perform a statistical approach by considering the redshifts of all potential host galaxies within the three-dimensional localization region of GW event to get a constraint on the distance-redshift relationship [1–3, 5]. However, our method can infer the

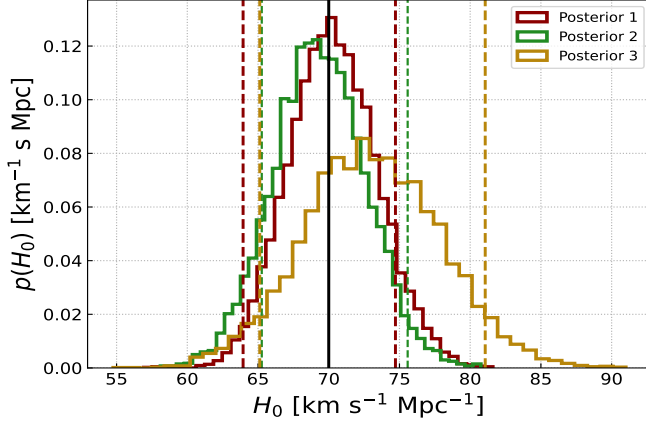


FIG. 6. Comparison of joint estimate of the Hubble constant over 50 GW events for the different choices of EoS. The black vertical line denotes the injected value of $H_0 = 70 \text{ km s}^{-1} \text{ Mpc}^{-1}$. The dashed vertical lines of the same color indicates 90% highest density credible interval corresponding to the histogram of that color.

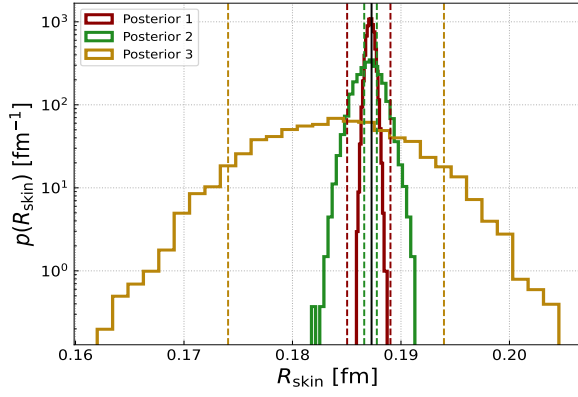


FIG. 7. Inferred posterior distributions of skin thickness for the different choices of the EoS priors. The black vertical line denotes the inferred value of the skin thickness $R_{\text{skin}} = 0.1873 \text{ fm}$ corresponding to injected EoS. The dashed vertical lines of the same color indicates 90% highest density credible interval corresponding to the histogram of that color.

redshift information of the GW event from the knowledge of the prior EoS parameters. We combine the redshift information with the luminosity distance measured from GW observation to estimate the Hubble constant.

We have tested our formalism using three different priors of the EoS parameters. We only infer the Hubble constant as the cosmological parameter in our Bayesian analysis. However, the methodology can also be extended to estimate other cosmological parameters, such as matter density and the dark energy equation of state. We can expect a significant constraint on the Hubble constant by 2nd generation detector era (see Ref. [2]). So, one can use constrained prior over the Hubble constant

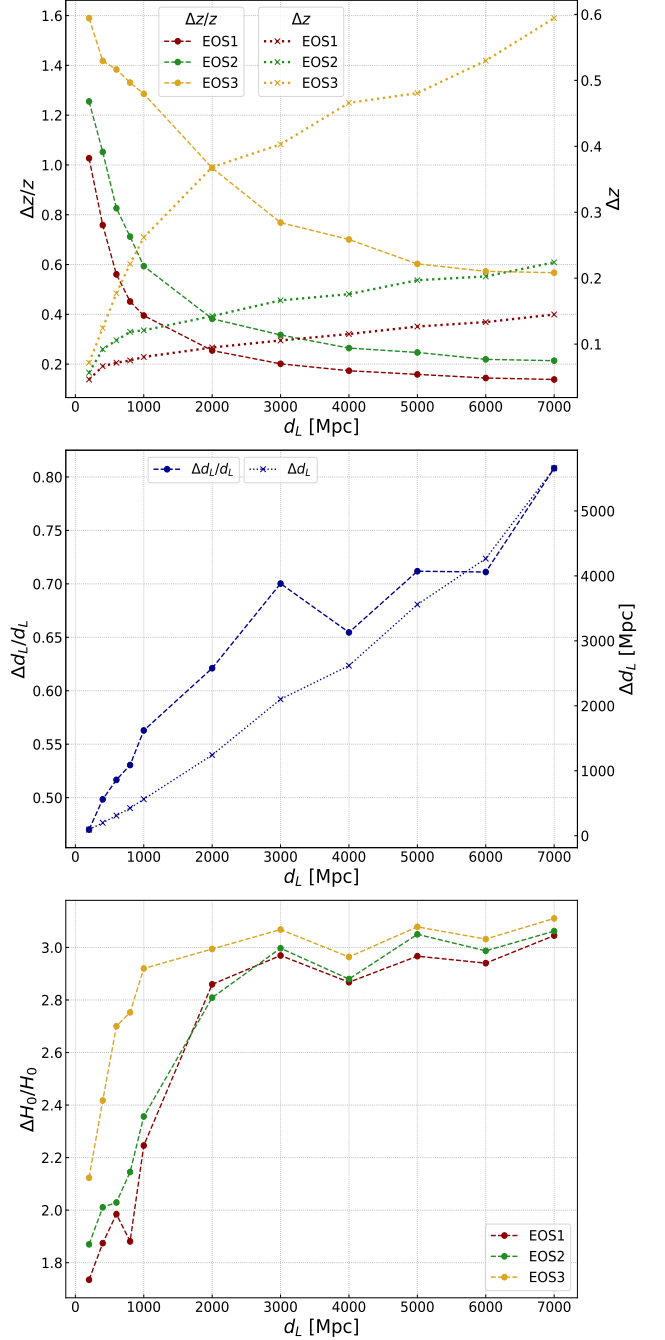


FIG. 8. Comparison of uncertainty in the measurement of z , d_L , and H_0 using a single BNS observation with source-frame mass pair $(1.4+1.26)M_\odot$ at different representative distances. *Top Panel*: Fractional uncertainty (left vertical axis) and uncertainty (right vertical axis) in the redshift measurement for three choices of EoS prior. *Middle Panel*: Fractional uncertainty (left vertical axis) and uncertainty (right vertical axis) in estimating luminosity distance from GW data. *Bottom Panel*: Fractional uncertainty of the Hubble constant for different EoS priors.

in 3rd detector era. The use of informed H_0 prior may help to estimate other cosmological parameters.

We can expect many detections of BNS mergers with 3rd generation detectors in the high redshift. We consider constant merger rate and a simple mass population model of BNS distribution in our work. However, we should consider a realistic merger rate (evolving with redshift) and population model of BNS distribution [57, 58]. Our methodology can easily be extended to incorporate simultaneous inference of other cosmological parameters and more realistic population models of NSs. We leave this work as a future exercise.

In the case of the EoS parameters, other observations can also put stringent measurements of the mass and radii of NSs. In particular, the observation of PSR J0030+0451 [41, 42] PSR J0740+6620 [43, 44] by NICER collaboration has been utilized to measure mass-radius relation of the NS.

ACKNOWLEDGEMENTS

We thank Rana Nandi and Prasanta Char for earlier collaboration (with BB and SB) on the construction of

the neutron star equation of state parameterization used here and for useful discussions. We would also like to thank Hsin-Yu Chen for carefully reading the manuscript and making several useful suggestions. TG gratefully acknowledges using the LDG clusters, Sarathi at IUCAA and Hawk at Cardiff University, accessed through the LIGO-Virgo-Kagra Collaboration. We are also grateful for the computational resource Pegasus provided by IUCAA for this work.

Appendix A: Bayesian Framework

From Bayes Theorem, the joint posterior of cosmological parameters and the EoS parameters for a detected GW event $p(H_0, \mathcal{E} | x_{\text{GW}})$ is given by

$$p(H_0, \mathcal{E} | x_{\text{GW}}) = p(x_{\text{GW}} | H_0, \mathcal{E})\pi(H_0)\pi(\mathcal{E}). \quad (\text{A1})$$

The likelihood for a single GW event in Eq. (A1) can be written as

$$p(x_{\text{GW}} | H_0, \mathcal{E}) \propto \frac{1}{\beta(H_0)} \iiint p(x_{\text{GW}_i} | m_1^z(m_1, z), m_2^z(m_2, z), \Lambda_1(m_1, \mathcal{E}), \Lambda_2(m_2, \mathcal{E}), d_L(z, H_0)) \times \pi(m_1, m_2)\pi(z)dzdm_1dm_2. \quad (\text{A2})$$

In terms of explicit parameters, Eq. (A) can conveniently be written as

$$p(x_{\text{GW}} | H_0, \mathcal{E}) = \frac{1}{\beta(H_0)} \iiint p(x_{\text{GW}_i} | z, m_1, m_2, \mathcal{E}, H_0) \times \pi(m_1, m_2)\pi(z)dzdm_1dm_2, \quad (\text{A3})$$

where a normalization term $\beta(H_0)$ has been included in the denominator to account for selection effects [2, 35].

$$\beta(H_0) = \int p_{\text{det}}(z, H_0)\pi(z)dz. \quad (\text{A4})$$

The term $p_{\text{det}}(z, H_0)$ in Eq. (A4) denotes detection probability for a particular choice of redshift and H_0 . We elaborate the calculation of $p_{\text{det}}(z, H_0)$ (similar to $p(d_{\text{GW}} | z, H_0)$ in Ref. [5]) following Gray *et al.* [5] (implemented in `gwcosmo`⁶).

The final joint posterior of the Hubble constant and the EoS parameters can be obtained by combining all sources, as follows:

$$p(H_0, \mathcal{E} | \{x_{\text{GW}}\}) = \prod_{i=1}^{N_{\text{det}}} p(H_0, \mathcal{E} | x_{\text{GW}_i}). \quad (\text{A5})$$

Appendix B: Estimation of Detection Probability

The selection effect as defined in Eq. (10) (also in Eq. (A4)) completely depends on GW detection efficiency. GW detector can identify those signals that generate sufficiently high amplitude response. We consider a GW event as detected if the network SNR is some threshold SNR ρ_{th} or higher. In our work, we set $\rho_{\text{th}} = 8$. We calculate p_{det} using the injection of BNS signal. We populate 10^3 BNSs uniformly over the entire sky for each of the redshift bin and a given choice of Hubble constant. These BNSs follow the same population model as we assumed for this work. We have injected the total number of BNS mergers $\sim 10^7$ for the entire range of the Hubble constant and redshift for computing detection probability; among all the sources, $\sim 8 \times 10^6$ sources qualify the detection criterion. We then calculate the matched filtering SNR [59] of the injected GW signal of 128s at each of the detector and hence the network SNR. For

⁶ gwcosmo code: <https://git.ligo.org/lscsoft/gwcosmo>

this purpose, we have used `bilby` [48] to inject GW signal and calculate the SNR. Since, ρ^2 follows non-central chi-squared distribution with two degrees of freedom [60], in the presence of stationary and Gaussian noise with a known power spectrum, we thus estimate the detection probability p_{det} for a certain redshift bin and a particular choice of H_0 by probability density function of non-

central chi-squared distribution with degrees of freedom is twice of the number of detectors and non-centrality parameter is ρ_{th} . The detection probability is estimated in the similar way as implemented in `gwcosmo`. Now, it is straight forward to calculate the selection function $\beta(H_0)$ (Eq. 10) by marginalizing the detection probability over the redshift prior used in the Bayesian framework.

-
- [1] B. F. Schutz, *Nature* **323**, 310 (1986).
- [2] H.-Y. Chen, M. Fishbach, and D. E. Holz, *Nature* **562**, 545 (2018), [arXiv:1712.06531 \[astro-ph.CO\]](#).
- [3] M. Fishbach *et al.* (LIGO Scientific, Virgo), *Astrophys. J. Lett.* **871**, L13 (2019), [arXiv:1807.05667 \[astro-ph.CO\]](#).
- [4] R. Nair, S. Bose, and T. D. Saini, *Phys. Rev. D* **98**, 023502 (2018), [arXiv:1804.06085 \[astro-ph.CO\]](#).
- [5] R. Gray *et al.*, *Phys. Rev. D* **101**, 122001 (2020), [arXiv:1908.06050 \[gr-qc\]](#).
- [6] S. Borhanian, A. Dhani, A. Gupta, K. G. Arun, and B. S. Sathyaprakash, *Astrophys. J. Lett.* **905**, L28 (2020), [arXiv:2007.02883 \[astro-ph.CO\]](#).
- [7] S. Bera, D. Rana, S. More, and S. Bose, *Astrophys. J.* **902**, 79 (2020), [arXiv:2007.04271 \[astro-ph.CO\]](#).
- [8] S. Mukherjee, B. D. Wandelt, S. M. Nissanke, and A. Silvestri, *Phys. Rev. D* **103**, 043520 (2021), [arXiv:2007.02943 \[astro-ph.CO\]](#).
- [9] B. P. Abbott *et al.* (LIGO Scientific, Virgo), *Phys. Rev. Lett.* **119**, 161101 (2017), [arXiv:1710.05832 \[gr-qc\]](#).
- [10] J. Aasi *et al.* (LIGO Scientific), *Class. Quant. Grav.* **32**, 074001 (2015), [arXiv:1411.4547 \[gr-qc\]](#).
- [11] F. Acernese *et al.* (VIRGO), *Class. Quant. Grav.* **32**, 024001 (2015), [arXiv:1408.3978 \[gr-qc\]](#).
- [12] B. P. Abbott *et al.* (LIGO Scientific, Virgo, 1M2H, Dark Energy Camera GW-E, DES, DLT40, Las Cumbres Observatory, VINROUGE, MASTER), *Nature* **551**, 85 (2017), [arXiv:1710.05835 \[astro-ph.CO\]](#).
- [13] M. Soares-Santos *et al.* (DES, Dark Energy Camera GW-EM), *Astrophys. J. Lett.* **848**, L16 (2017), [arXiv:1710.05459 \[astro-ph.HE\]](#).
- [14] R. Abbott *et al.* (LIGO Scientific, VIRGO, KAGRA), (2021), [arXiv:2111.03604 \[astro-ph.CO\]](#).
- [15] R. Abbott *et al.* (LIGO Scientific, VIRGO, KAGRA), (2021), [arXiv:2111.03606 \[gr-qc\]](#).
- [16] S. Mastrogiovanni, K. Leyde, C. Karathanasis, E. Chassande-Mottin, D. A. Steer, J. Gair, A. Ghosh, R. Gray, S. Mukherjee, and S. Rinaldi, *Phys. Rev. D* **104**, 062009 (2021), [arXiv:2103.14663 \[gr-qc\]](#).
- [17] B. P. Abbott *et al.* (LIGO Scientific, Virgo), *Astrophys. J.* **909**, 218 (2021), [arXiv:1908.06060 \[astro-ph.CO\]](#).
- [18] L. Verde, T. Treu, and A. G. Riess, *Nature Astron.* **3**, 891 (2019), [arXiv:1907.10625 \[astro-ph.CO\]](#).
- [19] N. Aghanim *et al.* (Planck), *Astron. Astrophys.* **641**, A6 (2020), [Erratum: *Astron. Astrophys.* 652, C4 (2021)], [arXiv:1807.06209 \[astro-ph.CO\]](#).
- [20] A. G. Riess *et al.*, (2021), [arXiv:2112.04510 \[astro-ph.CO\]](#).
- [21] C. Messenger and J. Read, *Phys. Rev. Lett.* **108**, 091101 (2012), [arXiv:1107.5725 \[gr-qc\]](#).
- [22] D. Chatterjee, A. H. K. R., G. Holder, D. E. Holz, S. Perkins, K. Yagi, and N. Yunes, *Phys. Rev. D* **104**, 083528 (2021), [arXiv:2106.06589 \[gr-qc\]](#).
- [23] K. Yagi and N. Yunes, *Class. Quant. Grav.* **33**, 13LT01 (2016), [arXiv:1512.02639 \[gr-qc\]](#).
- [24] B. Biswas, P. Char, R. Nandi, and S. Bose, *Phys. Rev. D* **103**, 103015 (2021), [arXiv:2008.01582 \[astro-ph.HE\]](#).
- [25] B. Biswas, *Astrophys. J.* **921**, 63 (2021), [arXiv:2105.02886 \[astro-ph.HE\]](#).
- [26] B. Biswas, R. Nandi, P. Char, S. Bose, and N. Stergioulas, *Mon. Not. Roy. Astron. Soc.* **505**, 1600 (2021), [arXiv:2010.02090 \[astro-ph.HE\]](#).
- [27] R. Gamba, J. S. Read, and L. E. Wade, *Class. Quant. Grav.* **37**, 025008 (2020), [arXiv:1902.04616 \[gr-qc\]](#).
- [28] B. Biswas, R. Nandi, P. Char, and S. Bose, *Phys. Rev. D* **100**, 044056 (2019), [arXiv:1905.00678 \[gr-qc\]](#).
- [29] G. Baym, C. Pethick, and P. Sutherland, *Astrophys. J.* **170**, 299 (1971).
- [30] W.-J. Xie and B.-A. Li, *Astrophys. J.* **883**, 174 (2019), [arXiv:1907.10741 \[astro-ph.HE\]](#).
- [31] M. Oertel, M. Hempel, T. Klöhn, and S. Typel, *Rev. Mod. Phys.* **89**, 015007 (2017), [arXiv:1610.03361 \[astro-ph.HE\]](#).
- [32] B. Biswas and S. Datta, (2021), [arXiv:2112.10824 \[astro-ph.HE\]](#).
- [33] M. Evans *et al.*, (2021), [arXiv:2109.09882 \[astro-ph.IM\]](#).
- [34] M. Maggiore *et al.*, *JCAP* **03**, 050 (2020), [arXiv:1912.02622 \[astro-ph.CO\]](#).
- [35] I. Mandel, W. M. Farr, and J. R. Gair, *Mon. Not. Roy. Astron. Soc.* **486**, 1086 (2019), [arXiv:1809.02063 \[physics.data-an\]](#).
- [36] B. P. Abbott *et al.* (LIGO Scientific, Virgo), *Class. Quant. Grav.* **37**, 045006 (2020), [arXiv:1908.01012 \[gr-qc\]](#).
- [37] K. Chatzioannou, *Gen. Rel. Grav.* **52**, 109 (2020), [arXiv:2006.03168 \[gr-qc\]](#).
- [38] J. Buchner, A. Georgakakis, K. Nandra, L. Hsu, C. Rangel, M. Brightman, A. Merloni, M. Salvato, J. Donley, and D. Kocevski, *Astron. Astrophys.* **564**, A125 (2014), [arXiv:1402.0004 \[astro-ph.HE\]](#).
- [39] S. Seabold and J. Perktold, in *9th Python in Science Conference* (2010).
- [40] R. Abbott *et al.* (LIGO Scientific, VIRGO, KAGRA), (2021), [arXiv:2111.03634 \[astro-ph.HE\]](#).
- [41] T. E. Riley *et al.*, *Astrophys. J. Lett.* **887**, L21 (2019), [arXiv:1912.05702 \[astro-ph.HE\]](#).
- [42] M. C. Miller *et al.*, *Astrophys. J. Lett.* **887**, L24 (2019), [arXiv:1912.05705 \[astro-ph.HE\]](#).
- [43] T. E. Riley *et al.*, *Astrophys. J. Lett.* **918**, L27 (2021), [arXiv:2105.06980 \[astro-ph.HE\]](#).
- [44] M. C. Miller *et al.*, *Astrophys. J. Lett.* **918**, L28 (2021), [arXiv:2105.06979 \[astro-ph.HE\]](#).
- [45] B. P. Abbott *et al.* (LIGO Scientific, Virgo), *Phys. Rev. Lett.* **121**, 161101 (2018), [arXiv:1805.11581 \[gr-qc\]](#).

- [46] B. P. Abbott, R. Abbott, T. D. Abbott, M. R. Abernathy, K. Ackley, C. Adams, P. Addesso, R. X. Adhikari, V. B. Adya, C. Affeldt, and et al., *Classical and Quantum Gravity* **34**, 044001 (2017).
- [47] T. Dietrich, A. Samajdar, S. Khan, N. K. Johnson-McDaniel, R. Dudi, and W. Tichy, *Phys. Rev. D* **100**, 044003 (2019), [arXiv:1905.06011 \[gr-qc\]](#).
- [48] G. Ashton, M. Hübner, P. D. Lasky, C. Talbot, K. Ackley, S. Biscoveanu, Q. Chu, A. Divakarla, P. J. Easter, B. Goncharov, and et al., *The Astrophysical Journal Supplement Series* **241**, 27 (2019).
- [49] P. Landry, R. Essick, and K. Chatziioannou, *Phys. Rev. D* **101**, 123007 (2020), [arXiv:2003.04880 \[astro-ph.HE\]](#).
- [50] C. Cutler and E. E. Flanagan, *Phys. Rev. D* **49**, 2658 (1994), [arXiv:gr-qc/9402014](#).
- [51] J. Aasi *et al.* (LIGO Scientific, VIRGO), *Phys. Rev. D* **88**, 062001 (2013), [arXiv:1304.1775 \[gr-qc\]](#).
- [52] J. Calderón Bustillo, S. H. W. Leong, T. Dietrich, and P. D. Lasky, *Astrophys. J. Lett.* **912**, L10 (2021), [arXiv:2006.11525 \[gr-qc\]](#).
- [53] D. Adhikari *et al.* (PREX), *Phys. Rev. Lett.* **126**, 172502 (2021), [arXiv:2102.10767 \[nucl-ex\]](#).
- [54] B. T. Reed, F. J. Fattoyev, C. J. Horowitz, and J. Piekarewicz, *Phys. Rev. Lett.* **126**, 172503 (2021), [arXiv:2101.03193 \[nucl-th\]](#).
- [55] J. Xu, W.-J. Xie, and B.-A. Li, *Phys. Rev. C* **102**, 044316 (2020), [arXiv:2007.07669 \[nucl-th\]](#).
- [56] X. Viñas, M. Centelles, X. Roca-Maza, and M. Warda, *Eur. Phys. J. A* **50**, 27 (2014), [arXiv:1308.1008 \[nucl-th\]](#).
- [57] J. Alsing, H. O. Silva, and E. Berti, *Mon. Not. Roy. Astron. Soc.* **478**, 1377 (2018), [arXiv:1709.07889 \[astro-ph.HE\]](#).
- [58] P. Landry and J. S. Read, *Astrophys. J. Lett.* **921**, L25 (2021), [arXiv:2107.04559 \[astro-ph.HE\]](#).
- [59] B. S. Sathyaprakash and B. F. Schutz, *Living Rev. Rel.* **12**, 2 (2009), [arXiv:0903.0338 \[gr-qc\]](#).
- [60] B. P. Abbott *et al.* (LIGO Scientific, Virgo), *Class. Quant. Grav.* **37**, 055002 (2020), [arXiv:1908.11170 \[gr-qc\]](#).